# Analyst

This is an *Accepted Manuscript*, which has been through the RSC Publishing peer review process and has been accepted for publication.

Accepted Manuscripts are published online shortly after acceptance, which is prior to technical editing, formatting and proof reading. This free service from RSC Publishing allows authors to make their results available to the community, in citable form, before publication of the edited article. This *Accepted Manuscript* will be replaced by the edited and formatted *Advance Article* as soon as this is available.

To cite this manuscript please use its permanent Digital Object Identifier (DOI®), which is identical for all formats of publication.

More information about *Accepted Manuscripts* can be found in the **Information for Authors**.
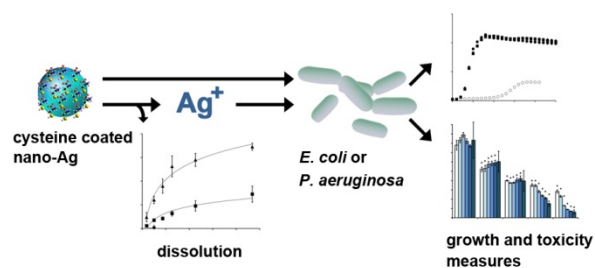
The toxicity of cysteine coated Ag nanoparticles to *E. coli* and *P. aeruginosa* was evaluated using an integrated approach that measured particle dissolution, bacterial growth, and effects on cell membranes.

1

2

3   Integrated Approach to Evaluating the Toxicity of Novel Cysteine-Capped Silver Nanoparticles

4   to *Escherichia coli* and *Pseudomonas aeruginosa*

5

6

7   John H. Priester[1,2,3], Aditi Singhal[3,4], Binghui Wu[4], Galen D. Stucky[3,4,5] and Patricia A.

8   Holden[1,2,3]*

9

10

11   [1]Bren School of Environmental Science & Management, [2]Earth Research Institute, [3]UC Center

12   for the Environmental Implications of Nanotechnology, [4]Department of Chemistry and

13   Biochemistry, [5]Materials Department, University of California, Santa Barbara, CA 93106

14

15

16

17   *Corresponding Author

18   Email: holden@bren.ucsb.edu

19   Tel: 805-893-3195

20   FAX: 805-893-7612

21

22   Running Title: Cysteine-capped Silver Nanoparticles and Bacteria

24 **ABSTRACT**

25 Because of microbial resistance to conventional antibiotics, there is increasing interest in silver,

26 including silver nanoparticles (nano-Ag), in antimicrobial applications. However, questions

27 remain regarding the relative roles of nano-Ag particles, versus Ag^+ ions released from nano-Ag

28 dissolution, in imparting bacterial toxicity. Here, we developed a novel nano-Ag that, based on

29 its cysteine cap, was expected to dissolve slowly and thus potentially allow for differentiating

30 nanoparticle, versus ionic, effects of Ag. The nano-Ag was systematically tested for its

31 differential toxicity to *Escherichia coli* and *Pseudomonas aeruginosa*. Bacterial growth, reactive

32 oxygen species (ROS) generation, particle dissolution, cellular electron transfer activity, and cell

33 membrane damage and potential were evaluated. In minimal growth medium, *E. coli* and *P.*

34 *aeruginosa* growth were slowed at 100 mg L^{-1} (0.93 mM) and 5 mg L^{-1} (0.046 mM),

35 respectively; *P. aeruginosa* was completely inhibited at and above 10 mg L^{-1} (0.093 mM). For

36 both strains, toxicity was associated with ROS and cell membrane damage. Based on

37 comparisons to $AgNO_3$ exposures, toxicity from nano-Ag was due to Ag^+ ions and not intact

38 nano-Ag, even though nanoparticle dissolution was less than 2% in minimal growth medium.

39 Because of their stability and slow Ag^+ ion release, the cysteine-capped nano-Ag particles here

40 are useful to antimicrobial applications. Additionally, our systematic approach to evaluating

41 toxicity, membrane damage, and ROS generation can be applied with other nanomaterials and

42 bacteria.

43

44

45

46

47   **INTRODUCTION**

48   Silver has long been used as an antimicrobial agent.[1] Its toxicity to microbes has been

49   attributed to cell membrane damage,[2,3] reactive oxygen species (ROS) generation with

50   subsequent oxidative damage,[4] DNA binding[5] and enzyme inactivation.[6,7] Interest in silver,

51   particularly in nanoscale applications, has increased as resistance to more conventional

52   antibiotics has occurred.[8]

53   Recently, nanoscale Ag (nano-Ag; defined as having at least one dimension <100 nm)

54   has been proposed for a wide variety of products and applications including water disinfection,[9]

55   and as a topical antibiotic.[10,11] Nano-Ag is attractive because of its demonstrated antibacterial,[12]

56   antiviral[13] and antifungal[14] activities. While the toxicity of nano-Ag to bacteria has been widely

57   reported,[15,16,17] the mechanisms of toxicity are not fully understood, including whether nano-Ag

58   is separately toxic compared to dissolved Ag ions.[18]

59   The susceptibility of bacteria to nano-Ag exposures is typically quantified in one of two

60   ways. In the first method, growth curves are generated by inoculating nano-Ag containing media

61   with bacteria (with no previous exposure) and tracking the population size through optical

62   density (OD) measurement.[17,19,20,21] In the second method, a healthy (usually exponential phase)

63   bacterial population is exposed to nano-Ag for a given time interval, a subsample of the

64   planktonic culture is spread onto solid growth medium, and the number of colony forming units

65   (CFUs) are counted over time.[2,6,16] While the latter method indicates the acute toxicity of the

66   particles, the former method better represents chronic exposures. Chronic exposures could be

67   useful in clinical applications; they are also environmentally-relevant, e.g. addressing general

68   concerns about engineered nanomaterials (ENMs) harming terrestrial[22,23,24] or aquatic[25,26]

69   ecosystems. Additionally, time-course growth data can be used in models describing ENM

70   toxicity, as has been demonstrated with *Pseudomonas aeruginosa* exposed to cadmium[27] and

71   CdSe quantum dots.[28]

72   ENM effects on bacterial growth may initiate at the bacterial cell envelope, where ENMs

73   first encounter bacteria and cause measurable physiological or morphological changes.[29] ROS

74   generation near the ENM-cell interface and consequent membrane damage have been well-

75   documented for CdSe QDs,[30] ZnO nanoparticles,[31] and Ag nanoparticles.[17] Silver/clay hybrid

76   nanoparticles induced time-dependent membrane disruption in *E. coli*.[32] Elevated intracellular

77   ROS levels rose in *E. coli*,[32] and in mixed-species nitrifying cultures isolated from activated

78   sludge in a wastewater treatment plant,[33] upon exposure to nano-Ag, potentially due to Ag

79   entering cells subsequent to membrane damage. Further, nano-Ag was shown to inactivate *E.*

80   *coli* membrane enzymes involved in electron transport,[34] and the membrane potential of *E. coli*

81   cells collapsed upon nano-Ag exposure.[21] Thus, ROS formation, membrane integrity, membrane

82   potential, and electron transport activity (a membrane function) are potentially altered by ENMs

83   including nano-Ag. However, their simultaneous relationship to bacterial growth is less

84   understood.

85   Previously, a system of bacterial toxicity assays was organized to assess abiotic and

86   biotic ROS, membrane integrity, membrane potential, and electron transport activity following

87   metal oxide nanomaterial exposure.[35] However, the assay results were not evaluated for their

88   relationship to bacterial population growth. Because many disease and ecosystem-level processes

89   are mostly occurring through bacterial population growth, it is important to assess growth effects

90   as possible consequences of nanomaterial impacts on bacterial membranes and membrane-

91   related processes. Here we evaluated nano-Ag toxicity to bacteria, by an approach integrated to

92   use acute membrane-related impacts to interpret longer-term population growth impacts. Growth

93   of *P. aeruginosa* and *E. coli* exposed to novel, cysteine-capped nano-Ag particles in minimal and

94   rich media was quantified. ROS (total and superoxide), membrane integrity, membrane potential

95   and membrane-associated electron transport activity were measured over time, following a short-

96   term exposure. The toxicity attributable to dissolved Ag was assessed through nano-Ag

97   dissolution experiments coupled with toxicity assessments using a silver salt ($AgNO_3$).

98   Measurements were made in 96-well microplates, which allows for adapting to high-throughput

99   systems.[36] Additionally, the combination of growth analysis, ROS generation measurement, and

100   cellular damage markers is suitable for use in predictive models that can better inform the

101   potential for environmental impacts.[37]

102

103   **EXPERIMENTAL SECTION**

104   **Chemicals and Nano-Ag Particles**

105   Unless otherwise noted, all chemicals were reagent grade or better (Sigma Chemical, St.

106   Louis, MO, USA; and Fisher Scientific, Hampton, NH, USA) and the water was nanopure (18

107   MΩ, Thermo Scientific Barnstead, Waltham, MA). Zheng *et al.*[38] reported the synthesis of

108   dodecanethiol-capped silver nanoparticles using benzene as the solvent. We modified the

109   synthesis procedure by varying the solvent, temperature and capping agent. L-cysteine (30.3

110   mg/0.25 mmol) was dissolved in 50-mL ethanol and 10-mL deionized water by continuous

111   stirring, followed by dissolving 85.0 mg (0.5 mmol) of $AgNO_3$ to obtain a cloudy yellow and

112   white solution. This solution was then heated under stirring at 55 ^{o}C for 10 min., followed by the

113   addition of 43.5 mg (0.5 mmol) of reducing agent *tert*-butylamine-borane complex (TBAB) and

114   keeping the solution stirring at 55 ^{o}C for 2 h. The solution was cooled to room temperature and

115   centrifuged to obtain a nanoparticle powder, which was dried under vacuum in a desiccator. The

116   particles obtained were black colored and dispersed in water. The particles were characterized by

117   several techniques, including ultraviolet–visible spectroscopy (UV-Vis), infrared spectroscopy

118   (IR), x-ray diffraction (XRD), scanning electron microscopy (SEM) and transmission electron

119   microscopy (TEM). Details on the particle characterization can be found in the Supporting

120   Information. To determine the average particle diameter, TEM micrographs were analyzed using

121   the Measurement Tool in Adobe Photoshop. A total of 75 individual nano-Ag particles were

122   measured for diameter. The hydrodynamic diameter (by dynamic light scattering) and zeta

123   potential of the nano-Ag particles at 10 mg L^{-1} (0.093 mM) were measured in H_2O and the

124   growth media (LB and MMD, as below) using a Malvern model Nano ZS90 Zeta Sizer

125   (Worcestershire, United Kingdom). Particle suspensions in the appropriate medium were

126   vortexed for 10 min prior to hydrodynamic diameter and zeta potential measurement. Prior to

127   bacterial experiments, the particles were stored as a powder in the dark at room temperature.

128

129   **Bacterial Strains and Inoculum Preparation**

130   *P. aeruginosa* strain PG201[30] and *E. coli* (ATTC 25922) were struck from frozen stock

131   (maintained at -80 ^{o}C in 70% Luria Bertani broth (LB) plus 30% glycerol) onto solid growth

132   medium (LB amended with 1.5% w/v agar) in separate Petri dishes, then incubated (30 ^{o}C, 18 h)

133   in the dark. One colony from each 18-h culture was dispersed into separate 4-mL volumes of

134   0.9% (w/v) NaCl solution to serve as the bacterial inoculum.

135

136   **Media Preparation and Bacterial Growth Measurements**

137   Bacterial growth experiments were performed in either nutrient rich (LB) or minimal

138   (Modified Minimal Davis; MMD, both at pH 7 as per Supporting Information for composition)

6

139   growth media. Each medium was amended with nano-Ag (synthesized as described above) and

140    $AgNO_3$ at varying total Ag concentrations (2.5, 5.0, 10.0 and 100.0 mg L^{-1}, or 0.023 mM, 0.046

141   mM, 0.093 mM and 0.93 mM, respectively); control medium preparations excluded Ag. For

142   preparing Ag-amended media, either particulate nano-Ag or $AgNO_3$ (3.0 mg and 4.7 mg for

143   nano-Ag and $AgNO_3$, respectively) was added to 30 mL of each medium type to achieve a total

144   Ag concentration of 100 mg L^{-1} (0.93 mM). The solutions were then vortexed for 10 min to

145   disperse the Ag, and diluted with sterile media to achieve the appropriate final concentration.

146   The Ag-amended media were transferred (200 µL per well) to 96-well plates (flat-bottomed

147   polystyrene with clear bottoms and sides; Corning Incorporated, MA, USA). Each treatment (i.e.

148   each medium type, for each Ag concentration) was added to a total of six wells: three for

149   inoculation, and three for uninoculated (abiotic) controls. Each plate well received 5 µL of the

150   inoculum described above, and plates were incubated (dark, 30° C, shaking at 200 rpm) in a

151   Synergy HT Multi-Mode microplate reader (Biotek Instruments, Winooski, VT, USA) equipped

152   with a xenon lamp set to measure optical density (600 nm, OD_{600}) regularly over time. Optical

153   density was recorded hourly for 24 h. Bacterial growth parameters (specific growth rate, lag time

154   and yield) were calculated as before.[30]

155

156   **Ag Dissolution**

157   The dissolution of nano-Ag (10 mg L^{-1} and 100 mg L^{-1}) and $AgNO_3$ (10 mg L^{-1}) in H_2O,

158   and MMD and LB media was evaluated over time using cellulose ester membrane (MWCO 100

159   kD) dialysis devices (Spectra/Por Float-A-Lyzer G2, Spectrum Labs, Rancho Dominguez, CA,

160   USA). A schematic of the dissolution experiment is shown in Figure S1. Solutions of nano-Ag

161   and $AgNO_3$ were prepared as described above from stored powders, and were immediately added

162   to sterile, acid washed glass test tubes at a volume of 44 mL. The dialysis devices, each

163   containing 6 mL of the appropriate medium (H_2O, MMD or LB), were then added to the test

164   tubes. Each treatment was prepared in triplicate. The tubes were incubated (30 ^{o}C, dark), and 0.2-

165   mL samples were aseptically removed from the inner volume at seven time points (0, 1, 2.5, 4.5,

166   6.5, 11.5 and 23.5 h). The samples were acidified (10% aqua regia, v/v) and the total Ag

167   concentration was measured by inductively coupled plasma atomic emission spectroscopy (ICP-

168   AES) using a TJA High Resolution IRIS instrument (Thermo Electron Corporation, Waltham,

169   MA, USA). Equilibrium silver speciation in MMD, assuming complete dissolution, was modeled

170   using MINEQL+ V:4.6 software (Environmental Research Software, Hallowell, ME, USA), as

171   detailed in the Supporting Information.

172

173   **Assays for ROS, Membrane Integrity, Electron Transfer Activity, and Membrane Potential**

174   Short term assays, recruited previously as a system for assessing effects of metal oxide

175   nanoparticles to bacteria,[35] were used to interpret the effects of Ag on bacterial growth. Since the

176   exact composition of LB is undefined, and interactions between medium components and Ag

177   may be difficult to quantify, we chose to conduct these short term assays only in MMD.

178   *E. coli* and *P. aeruginosa*, prepared as described above, were inoculated into 30 mL of

179   MMD then incubated at 30 ^{o}C (200 rpm, dark) until an OD_{600} of 0.1 was reached. To harvest

180   cells, the cultures were centrifuged (10k × g for 10 min) and the supernatant discarded. The

181   pellets were resuspended (by vortexing) in 15 mL of the growth medium. Quadruplicate 100-µL

182   culture aliquots, and quadruplicate abiotic controls (i.e. MMD without cells), were dispensed into

183   96-well plates for measuring ROS generation and cellular damage in the presence of Ag.

184   Separate plates were prepared for each of five assays: membrane integrity, membrane potential,

185   electron transport activity, total ROS concentration and superoxide concentration (Table S1).

186   The experimental details for the assays were identical to those previously used for metal oxide

187   nanoparticles,[35] with the exception that the superoxide assay was performed biotically rather than

188   abiotically, and total ROS was quantified both biotically and abiotically. Brief descriptions of

189   each assay can be found in the Supporting Information. For all of the assays, measurements were

190   made in the same microplate reader described above for the growth experiments. Where

191   applicable, the excitation wavelength was set to 485 nm. Mixtures (100 µL) of the assay reagents

192   and Ag (either nano-Ag or $AgNO_3$) were combined with the 100-µL cell culture aliquots. The

193   final (working) concentrations of Ag were 0, 2.5, and 10.0 mg L^{-1} (0, 0.023, and 0.093 mM,

194   respectively). Except when measurements were briefly made, the plates were continuously

195   incubated (30 ^{o}C) in the dark. The measurement intervals for each assay are shown in Table S1,

196   with time 0 occurring immediately after incubation. Abiotic signals (i.e. un-inoculated media

197   amended with either nano-Ag or $AgNO_3$) were subtracted from all biotic measurements to

198   account for any interferences of Ag with the assay reagents.

199

200   **Data and Statistical Analyses**

201   *E. coli* and *P. aeruginosa* specific growth rates were calculated from the slopes of linear

202   regression lines through log-transformed OD_{600} values plotted versus time, using Microsoft

203   Excel 2010 software as before.[39] Means were compared using Student's *t*-test or analysis of

204   variance (ANOVA). Relationships between the membrane integrity data and time were tested

205   with a two-way ANOVA.

206

207

208   **RESULTS AND DISCUSSION**

209   **Nano-Ag Characteristics and Dissolution**

210   The synthesis methods used herein resulted in uniformly-shaped (Figure 1) nano-Ag

211   (Figure S2) with a mean diameter of 9 nm (Figure S3). In H_2O, MMD and LB, the nano-Ag had

212   a mean hydrodynamic diameter of 58.8 nm, 24.5 nm and 27.5 nm, respectively. The mean zeta

213   potential of nano-Ag in H_2O, MMD and LB was -15.7 ± 0.3 mV, -18.1 ± 4.0 mV and -6.1 ± 1.0

214   mV, respectively. XRD analysis of the particles revealed a face centered cubic crystal structure

215   (Figure S4). Cysteine is known to readily bind Ag[40] at thiol groups,[41] and has been used to

216   mitigate the effects of Ag^+ ion toxicity to algae[42,43] and bacteria.[7] In the nano-Ag particles used

217   here the thiol group in cysteine (S-H) was altered to give an S-Ag bond, as indicated by Fourier

218   transform infrared spectroscopy (FTIR) (Figure S5). The strong bonding of cysteine to silver is

219   potentially useful for dispersing and stabilizing nano-Ag in aqueous environments, and for

220   slowing Ag^+ dissolution.

221   The nano-Ag particles at 10 mg L^{-1} and 100 mg L^{-1} dissolved somewhat in water and in

222   both growth media (Figure 2a-b), but the percent dissolution was very low compared to that of

223    $AgNO_3$ (100 mg L^{-1} only, Figure 2c). The dissolved ion concentration was lowest in H_2O, where

224    $< 1.5\%$ dissolution was measured at both nano-Ag concentrations (Figure 2a-b). Dissolved ion

225   concentrations were highest in LB, resulting in maximum percent dissolution values of $2.1\% \pm$

226   1.3% and $6.9\% \pm 0.3\%$ for 10 mg L^{-1} and 100 mg L^{-1} nano-Ag, respectively. These values

227   correspond to maximum Ag^+ ion concentrations of 0.21 ± 0.13 mg L^{-1} and 6.9 ± 0.3 mg L^{-1} for

228   the 10 mg L^{-1} and 100 mg L^{-1} nano-Ag treatments, respectively. Dissolution in MMD was 1.6%

229    $\pm 0.4\%$ (0.16 ± 0.04 mg L^{-1}) and $2.9\% \pm 0.7\%$ (2.9 ± 0.7 mg L^{-1}) for 10 mg L^{-1} and 100 mg L^{-1}

230   nano-Ag, respectively. In contrast, $AgNO_3$ dissolved completely in H_2O in approximately 10 h

231 (Figure 2c). AgNO$_3$ approached complete dissolution in LB (97.0% ± 2.4%), although this took

232 24 h. Dissolution in MMD reached a maximum of 56.3% ± 3.4%.

233 The dissolution percentages with our nano-Ag particles were similar to values presented

234 by others using organically coated nano-Ag, where less than 10% is typical.[43,44,45] Similarly, our

235 observed dissolution increase with ionic strength (LB > MMD) has been previously reported. For

236 example, Huynh and Chen[46] showed an increase in dissolution of citrate-capped nano-Ag from

237 approximately 4% in H$_2$O to 5% - 6% with varying concentrations of NaCl (455 mM), CaCl$_2$ (27

238 mM) and MgCl$_2$ (27 mM). The authors attributed this increase to the formation of silver chloride

239 complexes, which promotes the dissolution of nano-Ag.[47] Equilibrium chemical speciation

240 modeling (Table S2) of AgNO$_3$ and nano-Ag in MMD in the current experiment predicted the

241 presence of Ag$^+$ (89%), AgSO$_4^-$ (5%), AgNH$_3^+$ (5%) and Ag(NH$_3$)$_2^+$ (1%). Ag(OH)$_2^-$, AgOH and

242 AgNO$_3$ (for the AgNO$_3$ treatments only) were also predicted, but at concentrations < 0.1%.

243

244 **Bacterial Growth**

245 Both bacterial strains grew exponentially in each medium, but the lag times, growth rates,

246 and extent of growth varied by strain and by media. With, or without Ag amendment, growth in

247 MMD medium was reduced as compared to LB for both *E. coli* and *P. aeruginosa* (Figure S6,

248 Tables 1 and 2). Without Ag amendment, *E. coli* lag time increased 538% in MMD as compared

249 to LB, and the specific growth rate and maximum optical density decreased by 61% and 72%,

250 respectively (Table 1). Also in the absence of Ag, *P. aeruginosa* lag time increased 33% in

251 MMD as compared to LB, and specific growth rate and maximum optical density decreased by

252 40% and 87%, respectively. The reduction in growth is expected in the minimal medium as

253 compared to the complex, nutrient-rich LB. Wang and Koch[48] reported an approximately 57%

254 reduction in the growth rate of *E. coli* (calculated from optical density measurements) in a

255 minimal medium containing 0.2% glucose (comparable to the 0.3% used in the current study) as

256 compared to LB. A similar reduction in growth, as well as changes in gene expression patterns,

257 was demonstrated by *E. coli* in glucose-amended LB versus minimal media.[49]

258   Besides intrinsic effects of media, both *E. coli* and *P. aeruginosa* were more susceptible

259 to Ag toxicity in MMD as compared to LB. *E. coli* grew with $AgNO_3$ up to 10 mg L^{-1} in LB, but

260 was inhibited by $AgNO_3$ at all concentrations in MMD (Table 1, Figure S6b). In MMD, $AgNO_3$

261 inhibited *P. aeruginosa* growth at all concentrations, while growth in LB occurred up to 2.5 mg

262 L^{-1} (Table 2, Figure S6d).

263   Overall, nano-Ag was less toxic to bacterial growth as compared to $AgNO_3$ (Figure S6,

264 Tables 1 and 2), but the dose trends depended on bacterial strain and growth medium. For *E. coli*

265 in LB medium, bacterial growth metrics were similar for nano-Ag and $AgNO_3$ (Table 1).

266 However, for *P. aeruginosa* in LB, nano-Ag was much less growth inhibitory than $AgNO_3$

267 (Table 2).

268   When comparing within bacterial strain, but across growth media, *E. coli* cells grown in

269 MMD were more tolerant of nano-Ag than when grown in LB (Table 1). This is indicated by the

270 lack of *E. coli* growth at 100 mg mL^{-1} nano-Ag in LB, but only slightly reduced growth in MMD

271 at the same nano-Ag concentration (Table 1). In contrast, *E. coli* growth was previously reported

272 to be slowed, but not inhibited by, Ag nanoparticles at concentrations of $10 - 100$ mg L^{-1} in

273 LB.[17,50] Also, in minimal media, *E. coli* growth was slowed or inhibited by Ag nanoparticles at

274 concentrations less than 10 mg L^{-1}.[20,21,34,51] Thus, the relationship of media to nano-Ag impacts

275 on *E. coli* growth differ somewhat in our study as compared to other published reports.

276   Differently from *E. coli*, *P. aeruginosa* growth was more impacted by nano-Ag in MMD

277   than in LB (Table 2). In MMD, *P. aeruginosa* only tolerated nano-Ag up to 5 mg L^{-1} (Table 2).

278   When comparing across strains, with the exception of the 100 mg L^{-1} nano-Ag treatment in LB,

279   *E. coli* was more tolerant of Ag, as either AgNO$_3$ or nano-Ag, than *P. aeruginosa*. This is in

280   contrast to a prior report where *E. coli* appeared to be relatively more sensitive to Ag than *P.*

281   *aeruginosa*.[52]

282

283   **Assay Results for Total ROS and Superoxide**

284   As per the Methods, short term assays, previously recruited and tested as a system for

285   evaluating metal oxide nanomaterial effects on bacteria,[35] were used here to assess Ag impacts to

286   bacteria in MMD medium. Nano-Ag and AgNO$_3$ concentrations of 2.5 mg L^{-1} and 10 mg L^{-1}

287   were chosen for these assays because only *E. coli* was able to grow with 100 mg L^{-1} Ag (in

288   MMD).

289   In cell-free (abiotic) MMD, AgNO$_3$ resulted in time – dependent ROS generation, with

290   values of 204 ± 37 and 240 ± 35 mg L^{-1} H$_2$O$_2$ equivalents for the 2.5 mg L^{-1} and 10 mg L^{-1}

291   treatments, respectively, after 60 min. For 2.5 mg L^{-1} and 10 mg L^{-1} of nano-Ag, ROS levels

292   were 0 and 92 ± 18 mg L^{-1} H$_2$O$_2$ equivalents, respectively, after 60 min. There was a hyperbolic

293   relationship between total abiotic ROS and Ag$^+$ ion concentration in solution after 60 min.

294   (Figure S7). In *E. coli* suspensions after 60 min. of exposure, ROS (cellular) was only detected

295   with AgNO$_3$ (Table S3). Cellular ROS levels after 60 min. in *P. aeruginosa* cultures were

296   elevated upon exposure to Ag in both forms, with values being highest for AgNO$_3$ (Table S3).

297   In both the *E. coli* and *P. aeruginosa* suspensions, superoxide was not detected. Ivask *et*

298   *al.*[53] reported intracellular superoxide production in *E. coli* exposed to silver nanoparticles and

13

299   AgNO$_3$ at low exposure concentrations (< 1 mg L^{-1}). Their superoxide measurement protocol

300   used a bioluminescent *E. coli* reporter strain, which may have been more sensitive than the XTT

301   assay used here. Additionally, it took 5 hours of exposure to detect superoxide, which was longer

302   than the 4-hour exposure here.

303   ROS generation by silver has been documented,[4,16] and ROS has been implicated in the

304   toxicity of silver nanoparticles to bacteria. Choi and Hu[33] used the DCFH-DA assay to

305   demonstrate both abiotic and intracellular ROS production in nitrifying bacteria exposed to silver

306   nanoparticles and ions at concentrations of 1 mg L^{-1} or less. Intracellular ROS levels correlated

307   with silver nanoparticle toxicity. Interestingly, AgNO$_3$ did not result in higher ROS levels than

308   the nanoparticles,[33] which contrasts to our results herein. Particle dissolution in the exposure

309   medium was not evaluated, however, so it is possible that complete dissolution occurred,

310   resulting in the similar results for silver nanoparticles and AgNO$_3$.[33] Su *et al.*[32] showed an

311   increase in ROS levels, as quantified by the DCFH-DA assay, when *E. coli* was exposed to

312   silver/clay nanoparticle hybrids (ca. 30 mg L^{-1} silver) for 2 h.

313

314   **Assay Results for Membrane Integrity, Electron Transport Activity, and Membrane**

315   **Potential plus Relationships to ROS and Ag$^+$ Ion Concentrations**

316   *E. coli* membrane integrity appeared to decrease over time upon exposure to AgNO$_3$

317   (Figure 3a), with 38% and 79% reductions in green:red fluorescence for the 2.5 mg L^{-1} and 10

318   mg L^{-1} treatments after 4 h, respectively, as compared to the control. Nano-Ag exposure did not

319   reduce membrane integrity in *E. coli* (Figure 3a). In *P. aeruginosa*, membrane integrity

320   decreased in most silver treatments relative to the control (Figure 3b). Green:red fluorescence

321   appeared to be more decreased in AgNO$_3$ than nano-Ag treatments, with 82% and 93%

322   reductions (as compared to the control) after 4 h of exposure for the 2.5 mg L^{-1} and 10 mg L^{-1}

323   concentrations, respectively (Figure 3b). With nano-Ag, green:red fluorescence was decreased

324   by 28% and 54% at 2.5 mg L^{-1} and 10 mg L^{-1}, respectively. Membrane integrity reduction

325   increased with increasing ROS (Figure 4a) and Ag^+ ion concentration (Figure 4b), with the

326   effects being more pronounced in *P. aeruginosa* than *E. coli*.

327   Membrane integrity, as quantified by SYTO 9:propidium iodide fluorescence, has

328   previously been evaluated upon silver nanoparticle exposure. Choi *et al.*[51] did not observe

329   changes in the membrane integrity of either *E. coli* or enriched nitrifying cultures exposed to Ag

330   nanoparticles or Ag^+ ions at 1 mg L^{-1}. It is possible that those exposure times were too short,

331   however, as we did not observe changes in *E. coli* membrane integrity during less than 2 hours of

332   exposure (i.e., the approximate doubling time of *E. coli* in MMD media without Ag amendment,

333   Table 1). Su *et al.*[32] observed membrane disruption in *E. coli* during exposure to silver/clay

334   nanoparticle hybrids (ca. 30 mg L^{-1} silver) over 24 – 72 h. *E. coli* membrane disruption was

335   associated with intracellular ROS production,[32] which also appears to be the case here. At 1 h of

336   exposure, membrane integrity disruption was increased according to total ROS concentration

337   (Figure 4a), i.e. the ROS produced within the medium. The effect also occurred for *P.*

338   *aeruginosa*, where there was a significant correlation between membrane integrity disruption and

339   total abiotic ROS (ANOVA, $p = 0.03$). However, cellular ROS are produced, and scavenged,

340   during normal oxidative metabolism. Thus, the insignificant levels of cellular ROS for *E. coli*

341   exposed to nano-Ag (Table S3) are consistent with normal growth in MMD (Figure S6a, Table

342   1), by presumably normally-metabolizing cells. That the cellular ROS was very high in *E. coli*

343   exposed to $AgNO_3$ in MMD (Table S3) while its growth rate was insignificant (Table 1) may

344   point to either excessive cellular ROS production, inefficient scavenging, or both. *P. aeruginosa*

345 cellular ROS was similarly high for the $AgNO_3$ and nano-Ag treatments in MMD (Table S3),

346 and growth was impaired (Table 2, Figure S6c,d), consistent with relatively impaired membrane

347 integrity (Figure 3) and similarly high abiotic (thus, extracellular) ROS levels (Figure 4).

348   Comparatively, although cellular ROS levels were higher in *E. coli* as compared to *P.*

349 *aeruginosa* (Table S3), there was less membrane damage and toxicity. *E. coli* appeared to have

350 been more resistant to Ag-induced membrane damage, and thus grew more (as above) as

351 compared to *P. aeruginosa*. The increase in Ag susceptibility in *P. aeruginosa* may be related to

352 inherent membrane permeability differences. Fukuoka *et al.*[54] reported increased antibiotic

353 transport across *P. aeruginosa* membranes in a minimal medium, leading to enhanced toxicity.

354 The increased permeability was attributed to a lack of competitive inhibition at a protein channel

355 in the low amino acid medium, allowing for more antibiotic transport.[54]

356   In addition to membrane integrity, membrane potential was measured by $DiOC_2$, which

357 enters cells with established potentials and shifts from green to red fluorescence as the dye

358 molecules self-associate. With a compromised membrane potential, the red:green fluorescence is

359 reduced, as was observed with *E. coli* exposed to 10 mg L^{-1} $AgNO_3$ (Figure S8a). A similar

360 dissipation in *E. coli* membrane potential was observed by Lok *et al.*[21] upon silver nanoparticle

361 or $AgNO_3$ exposure. The collapse of the potential was attributed to K^+ ion leakage into the

362 extracellular environment due to membrane damage. Ag^+ ions were also shown to cause massive

363 proton leakage, and the subsequent collapse of membrane potential, in *Vibrio cholerae*

364 membrane vesicles.[55] Proton leakage was attributed to the alteration of membrane protein

365 structure, or membrane damage. This is consistent with our *E. coli* results for 10 mg L^{-1} $AgNO_3$

366 exposure, where there was a simultaneous reduction in both membrane integrity and membrane

367 potential. The results for *P. aeruginosa* differed from *E. coli*, as exposure to $AgNO_3$ at both 2.5

16

368   and 10 mg L^{-1} caused an increase in red:green fluorescence relative to the control (Figure S8b).

369   This may have been caused by acute membrane permeabilization (Figure 3), which not only

370   would have collapsed the membrane potential, but also would have allowed DiOC$_2$ to freely

371   diffuse into the cell independent of potential, causing an increase in red fluorescence.

372   Electron transport chain function was quantified using the commercial RedoxSensor

373   Green dye. This dye penetrates all cells, and is reduced in the presence of a functional electron

374   transport chain, forming a fluorescent compound. A reduction in green fluorescence indicates

375   limited electron transport chain function. In both *E. coli* and *P. aeruginosa*, green fluorescence

376   was reduced as compared to controls in the presence of AgNO$_3$, with the effect being greatest at

377   10 mg L^{-1} (Figure S9). In the presence of nano-Ag, however, green fluorescence increased for

378   both *E. coli* and *P. aeruginosa* (Figure S9). The RedoxSensor Green dye directly measures

379   bacterial reductase (namely dehydrogenase) activity, which in turn is a proxy for electron

380   transport function. Li *et al.*[34] reported the inhibition of *E. coli* dehydrogenase upon exposure to

381   50 mg L^{-1} of silver nanoparticles. Five (5) mg L^{-1} also inhibited dehydrogenase activity, but

382   initial time points showed an increase in activity as compared to controls; a similar trend to what

383   was observed in the present work. Xiu *et al.*[18] reported stimulation of *E. coli* survival upon

384   exposure to sub-lethal Ag$^+$ ion concentrations, although the mechanism for increased survival

385   was unknown. It is possible that reductase activity was stimulated in the presence of nano-Ag,

386   although this phenomenon was not further evaluated here. Another possibility is that the increase

387   in green fluorescence is an artifact of the nano-Ag used here, as it has been reported that cysteine

388   can influence the measurement of bacterial redox reactions.[56]

389

390   **Ag$^+$ Ion versus Nano-Ag Effects**

391   Understanding ion release is critical when evaluating the toxicity of nanomaterials.[57] In

392   certain scenarios, ions and intact particles each contribute to measured toxicity. Mammalian cells

393   exposed to nano-Ag resulted in morphological changes not observed with ionic Ag.[58] In a study

394   of *P. aeruginosa* exposed to CdSe quantum dots (QDs), specific growth rates were equally

395   impaired by Cd^{2+} and CdSe up to a QD concentration of 50 mg L^{-1}, after which the specific

396   growth rates decreased more rapidly upon QD exposure, suggesting that toxicity depended on the

397   presence of intact particles as opposed to dissolved ions.[30] Similar plots of the current data

398   (Figure 5), using the measured dissolution of nano-Ag and $AgNO_3$ at 6 h, do not show this

399   phenomenon. In both LB (Figure 5a) and MMD (Figure 5b), nano-Ag and $AgNO_3$ data points

400   overlap, indicating an Ag^+ ion-dependent reduction in specific growth rate independent of the

401   form of Ag delivery. Consistent with the growth metrics described above, specific growth rate

402   decreased more rapidly with increasing Ag^+ ion concentration in MMD as compared to LB, and

403   specific growth rates in both media were more negatively correlated with Ag^+ ion concentration

404   for *P. aeruginosa* than *E. coli*. Thus, although Ag appeared to be more soluble in LB than in

405   MMD (Figure 2), toxicity was greater in MMD. This could be explained if silver-binding ligands

406   are present in LB and not MMD, thus reducing the bioavailability of Ag^+ ions. In a study of *E.*

407   *coli* grown in LB it was shown that several amino acid metabolites were present, including thiols

408   such as cysteine that have a high affinity for Ag.[59] Such metabolites could bind Ag^+ ions

409   dissolved from nano-Ag or $AgNO_3$, effectively reducing cellular exposure.

410   Others have also shown that nano-Ag toxicity can be solely attributed to Ag^+ ion

411   release.[18,45] Ag^+ ion release from nano-Ag occurs by oxidation at the particle surfaces.[60,61] Xiu *et*

412   *al.*[18] demonstrated the mitigation of nano-Ag toxicity to *E. coli* under anaerobic conditions,

413   where the absence of O_2 prevented surface oxidation and ion release. Similarly, nano-Ag toxicity

414 to *Caenorhabditis elegans* was caused by Ag^+ ion release.[45] Cysteine is believed to slow Ag^+ ion

415 release from nano-Ag by binding to the particle surface and inhibiting O_2 attachment, which is

416 required for oxidation.[62] This phenomenon is of potential interest in the design of nano-Ag for

417 clinical purposes, where a controlled release of Ag^+ ions is desired. Additionally, the interaction

418 of nano-Ag and cysteine is of environmental relevance, as these particles may encounter cysteine

419 or other thiol ligands upon release into aquatic or soil ecosystems. Gondikas *et al.*[44]

420 demonstrated cysteine adsorption to, and increased dissolution and aggregation of, citrate and

421 PVP-capped nano-Ag, potentially changing the bioavailability of these particles. Thus the

422 cysteine-capped nano-Ag particles used in the present work are of clinical and environmental

423 interest when evaluating toxicity to bacteria.

424

425 **CONCLUSIONS**

426   In this work we employed a comprehensive set of membrane damage-related assays,

427 along with measurements of growth, to assess cysteine-capped silver nanoparticle toxicity to

428 bacteria. While bacterial growth or killing measurements are valuable in evaluating the

429 effectiveness of ENMs as antimicrobial agents, they do not directly explain the observed

430 toxicity. Simultaneously measuring growth, ROS generation, membrane damage, electron

431 transport activity, and membrane potential, as was done in this work, gives a more complete

432 understanding of how ENMs impart toxicity. Combining these measurements with evaluations of

433 particle dissolution, and comparisons to dissolved ion toxicity, gives further information on the

434 causes of observed ENM effects.

435   The results presented here highlight the importance of Ag^+ ion dissolution, with

436 subsequent ROS generation and membrane damage, in initiating the toxicity of nano-Ag to

437   bacteria. The measured nano-Ag toxicity to *E. coli* and *P. aeruginosa* was explainable by particle

438   dissolution alone: Ag^+ ion concentration was positively correlated with reduced membrane

439   integrity which was well correlated, particularly for *P. aeruginosa* which appeared to be

440   hypersensitive to Ag toxicity, with growth rate reduction. The novel cysteine-capped nano-Ag

441   particles used in this work have potential use in antimicrobial applications because of their

442   stability and slow dissolution in aqueous environments. Additionally, the results presented here

443   provide insight on the potential effects of released nano-Ag, as toxicity in the environment may

444   be mitigated by the acquisition of coatings such as cysteine that slow or prevent particle

445   dissolution.

446

456

457   **REFERENCES**
458

459   1.   H. J. Klasen, *Burns*, 2000, **26**, 117-130.

460   2.   W. K. Jung, H. C. Koo, K. W. Kim, S. Shin, S. H. Kim and Y. H. Park, *Appl. Environ. Microbiol.*, 2008,
461   **74**, 2171-2178.

20

Analyst Accepted Manuscript

462   3.   Q. L. Feng, J. Wu, G. Q. Chen, F. Z. Cui, T. N. Kim and J. O. Kim, *J. Biomed. Mater. Res.*, 2000, **52**,
463   662-668.

464   4.   H.-J. Park, J. Y. Kim, J. O. Kim, J.-H. Lee, J.-S. Hahn, M. B. Gu and J. Yoon, *Water Res.*, 2009, **43**,
465   1027-1032.

466   5.   H. Arakawa, J. F. Neault and H. A. Tajmir-Riahi, *Biophys. J.*, 2001, **81**, 1580-1587.

467   6.   M. Yamanaka, K. Hara and J. Kudo, *Appl. Environ. Microbiol.*, 2005, **71**, 7589-7593.

468   7.   S. Y. Liau, D. C. Read, W. J. Pugh, J. R. Furr and A. D. Russell, *Lett. Appl. Microbiol.*, 1997, **25**, 279-
469   283.

470   8.   D. M. Aruguete, B. Kim, M. F. Hochella, Jr., Y. Ma, Y. Cheng, A. Hoegh, J. Liu and A. Pruden,
471   *Environ. Sci.: Processes Impacts*, 2013, **15**, 93-102.

472   9.   Q. Li, S. Mahendra, D. Y. Lyon, L. Brunet, M. V. Liga, D. Li and P. J. J. Alvarez, *Water Res.*, 2008,
473   **42**, 4591-4602.

474   10.   M. K. Rai, A. Yadav and A. K. Gade, *Biotechnol. Adv.*, 2009, **27**, 76-83.

475   11.   I. Chopra, *J. Antimicrob. Chemoth.*, 2007, **59**, 587-590.

476   12.   M. K. Rai, S. D. Deshmukh, A. P. Ingle and A. K. Gade, *J. Appl. Microbiol.*, 2012, **112**, 841-852.

477   13.   J. V. Rogers, C. V. Parkinson, Y. W. Choi, J. L. Speshock and S. M. Hussain, *Nanoscale Res. Lett.*,
478   2008, **3**, 129-133.

479   14.   I.-S. Hwang, J. Lee, J. H. Hwang, K.-J. Kim and D. G. Lee, *Febs J.*, 2012, **279**, 1327-1338.

480   15.   C. Marambio-Jones and E. M. V. Hoek, *J. Nanopart. Res.*, 2010, **12**, 1531-1551.

481   16.   J. S. Kim, E. Kuk, K. N. Yu, J.-H. Kim, S. J. Park, H. J. Lee, S. H. Kim, Y. K. Park, Y. H. Park, C.-Y.
482   Hwang, Y.-K. Kim, Y.-S. Lee, D. H. Jeong and M.-H. Cho, *Nanomed.-Nanotechnol.*, 2007, **3**, 95-
483   101.

484   17.   I. Sondi and B. Salopek-Sondi, *J. Colloid Interf. Sci.*, 2004, **275**, 177-182.

485   18.   Z.-M. Xiu, Q.-B. Zhang, H. L. Puppala, V. L. Colvin and P. J. J. Alvarez, *Nano Lett.*, 2012, **12**, 4271-
486   4275.

487   19.   M. Raffi, F. Hussain, T. M. Bhatti, J. I. Akhter, A. Hameed and M. M. Hasan, *J. Mater. Sci.*
488   *Technol.*, 2008, **24**, 192-196.

489   20.   S. K. Gogoi, P. Gopinath, A. Paul, A. Ramesh, S. S. Ghosh and A. Chattopadhyay, *Langmuir*, 2006,
490   **22**, 9322-9328.

491   21.   C. N. Lok, C. M. Ho, R. Chen, Q. Y. He, W. Y. Yu, H. Z. Sun, P. K. H. Tam, J. F. Chiu and C. M. Che, *J.*
492   *Proteome Res.*, 2006, **5**, 916-924.

493   22.   Y. Ge, J. P. Schimel and P. A. Holden, *Appl. Environ. Microb.*, 2012, **78**, 6749-6758.

494   23.   J. H. Priester, Y. Ge, R. E. Mielke, A. M. Horst, S. C. Moritz, K. Espinosa, J. Gelb, S. L. Walker, R. M.
495   Nisbet, Y.-J. An, J. P. Schimel, R. G. Palmer, J. A. Hernandez-Viezcas, L. Zhao, J. L. Gardea-
496   Torresdey and P. A. Holden, *Proc. Natl. Acad. Sci. USA*, 2012, **109**, E2451-E2456.

497   24.   Y. Ge, J. P. Schimel and P. A. Holden, *Environ. Sci. Technol.*, 2011, **45**, 1659-1664.

498   25.   T. A. Jarvis, R. J. Miller, H. S. Lenihan and G. K. Bielmyer, *Environ. Toxicol. Chem.*, 2013, **32**, 1264-
499   1269.

500   26.   A. A. Keller, K. Garner, R. J. Miller and H. S. Lenihan, *Plos One*, 2012, **7**, e43983.

501   27.   T. Klanjscek, R. M. Nisbet, J. H. Priester and P. A. Holden, *Plos One*, 2012, **7**, e26955.

502   28.   T. Klanjscek, R. M. Nisbet, J. H. Priester and P. A. Holden, *Ecotoxicology*, 2013, **22**, 319-330.

503   29.   W. Jiang, K. Yang, R. W. Vachet and B. Xing, *Langmuir*, 2010, **26**, 18071-18077.

504   30.   J. H. Priester, P. K. Stoimenov, R. E. Mielke, S. M. Webb, C. Ehrhardt, J. P. Zhang, G. D. Stucky and
505   P. A. Holden, *Environ. Sci. Technol.*, 2009, **43**, 2589-2594.

506   31.   Z. Huang, X. Zheng, D. Yan, G. Yin, X. Liao, Y. Kang, Y. Yao, D. Huang and B. Hao, *Langmuir*, 2008,
507   **24**, 4140-4144.

508   32.   H.-L. Su, C.-C. Chou, D.-J. Hung, S.-H. Lin, I. C. Pao, J.-H. Lin, F.-L. Huang, R.-X. Dong and J.-J. Lin,
509   *Biomaterials*, 2009, **30**, 5979-5987.

510   33.   O. Choi and Z. Hu, *Environ. Sci. Technol.*, 2008, **42**, 4583-4588.

511   34.   W.-R. Li, X.-B. Xie, Q.-S. Shi, H.-Y. Zeng, Y.-S. Ou-Yang and Y.-B. Chen, *Appl. Microbiol. Biot.*, 2010,
512   **85**, 1115-1122.

513   35.   A. M. Horst, R. Vukanti, J. H. Priester and P. A. Holden, *Small*, 2013, **9**, 1753-1764.

514   36.   X. Jin, M. Li, J. Wang, C. Marambio-Jones, F. Peng, X. Huang, R. Damoiseaux and E. M. V. Hoek,
515   *Environ. Sci. Technol.*, 2010, **44**, 7321-7328.

516   37.   P. A. Holden, R. M. Nisbet, H. S. Lenihan, R. J. Miller, G. N. Cherr, J. P. Schimel and J. L. Gardea-
517   Torresdey, *Acc. Chem. Res.*, 2013, **46**, 813-822.

518   38.   N. Zheng, J. Fan and G. D. Stucky, *J. Am. Chem. Soc.*, 2006, **128**, 6550-6551.

519 39. R. E. Mielke, J. H. Priester, R. A. Werlin, J. Gelb, A. M. Horst, E. Orias and P. A. Holden, *Appl.*
520   *Environ. Microbiol.*, 2013, **79**, 5616-5624.

521 40. L.-O. Andersson, *J. Polym. Sci. A1*, 1972, **10**, 1963-1973.

522 41. R. A. Bell and J. R. Kramer, *Environ. Toxicol. Chem.*, 1999, **18**, 9-22.

523 42. A.-J. Miao, K. A. Schwehr, C. Xu, S.-J. Zhang, Z. Luo, A. Quigg and P. H. Santschi, *Environ. Pollut.*,
524   2009, **157**, 3034-3041.

525 43. E. Navarro, F. Piccapietra, B. Wagner, F. Marconi, R. Kaegi, N. Odzak, L. Sigg and R. Behra,
526   *Environ. Sci. Technol.*, 2008, **42**, 8959-8964.

527 44. A. P. Gondikas, A. Morris, B. C. Reinsch, S. M. Marinakos, G. V. Lowry and H. Hsu-Kim, *Environ.*
528   *Sci. Technol.*, 2012, **46**, 7037-7045.

529 45. X. Yang, A. P. Gondikas, S. M. Marinakos, M. Auffan, J. Liu, H. Hsu-Kim and J. N. Meyer, *Environ.*
530   *Sci. Technol.*, 2012, **46**, 1119-1127.

531 46. K. A. Huynh and K. L. Chen, *Environ. Sci. Technol.*, 2011, **45**, 5564-5571.

532 47. X. Li, J. J. Lenhart and H. W. Walker, *Langmuir*, 2010, **26**, 16690-16698.

533 48. C. H. Wang and A. L. Koch, *J. Bacteriol.*, 1978, **136**, 969-975.

534 49. H. Tao, C. Bausch, C. Richmond, F. R. Blattner and T. Conway, *J. Bacteriol.*, 1999, **181**, 6425-6440.

535 50. A. Dror-Ehre, H. Mamane, T. Belenkova, G. Markovich and A. Adin, *J. Colloid Interf. Sci.*, 2009,
536   **339**, 521-526.

537 51. O. Choi, K. K. Deng, N.-J. Kim, L. Ross, Jr., R. Y. Surampalli and Z. Hu, *Water Res.*, 2008, **42**, 3066-
538   3074.

539 52. J. R. Morones, J. L. Elechiguerra, A. Camacho, K. Holt, J. B. Kouri, J. T. Ramirez and M. J. Yacaman,
540   *Nanotechnology*, 2005, **16**, 2346-2353.

541 53. A. Ivask, O. Bondarenko, N. Jepihhina and A. Kahru, *Anal. Bioanal. Chem.*, 2010, **398**, 701-716.

542 54. T. Fukuoka, N. Masuda, T. Takenouchi, N. Sekine, M. Iijima and S. Ohya, *Antimicrob. Agents Ch.*,
543   1991, **35**, 529-532.

544 55. P. Dibrov, J. Dzioba, K. K. Gosink and C. C. Hase, *Antimicrob. Agents Ch.*, 2002, **46**, 2668-2670.

545 56. J. Green and M. S. Paget, *Nat. Rev. Microbiol.*, 2004, **2**, 954-966.

546 57. S. K. Misra, A. Dybowska, D. Berhanu, S. N. Luoma and E. Valsami-Jones, *Sci. Total Environ.*,
547   2012, **438**, 225-232.

548   58.   K. Kawata, M. Osawa and S. Okabe, *Environ. Sci. Technol.*, 2009, **43**, 6046-6051.

549   59.   G. Sezonov, D. Joseleau-Petit and R. D'Ari, *J. Bacteriol.*, 2007, **189**, 8746-8749.

550   60.   J. Liu and R. H. Hurt, *Environ. Sci. Technol.*, 2010, **44**, 2169-2175.

551   61.   C.-N. Lok, C.-M. Ho, R. Chen, Q.-Y. He, W.-Y. Yu, H. Z. Sun, P. K.-H. Tam, J.-F. Chiu and C.-M. Che,
552   *J. Biol. Inorg. Chem.*, 2007, **12**, 527-534.

553   62.   J. Liu, D. A. Sonshine, S. Shervani and R. H. Hurt, *ACS Nano*, 2010, **4**, 6903-6913.

554

555

24

LIST OF TABLES AND FIGURES

Table 1. Growth parameters for *E. coli* cultures exposed to varying nano-Ag and AgNO$_3$ concentrations. NG denotes no growth, thus the parameters could not be calculated for these treatments. Like letters in each column indicate no significant difference (t – test, p > 0.05).

Medium: LB, Ag Type: nano-Ag			
Concentration (mg/L)	Lag Time (h)	Specific Growth Rate (h^{-1})	Max. OD$_{600}$
0	1.16 ± 0.21^a	0.98 ± 0.01^a	1.27 ± 0.03^a
2.5	0.56 ± 0.11^b	0.90 ± 0.01^b	1.10 ± 0.00^b
5.0	0.38 ± 0.16^b	0.91 ± 0.00^b	$1.10 \pm 0.01^{b,c}$
10.0	0.59 ± 0.06^b	0.90 ± 0.00^b	1.09 ± 0.01^c
100.0	NG	NG	NG
Medium: LB, Ag Type: AgNO$_3$			
Concentration (mg/L)	Lag Time (h)	Specific Growth Rate (h^{-1})	Max. OD$_{600}$
0	1.16 ± 0.21^a	0.98 ± 0.01^a	1.27 ± 0.03^a
2.5	0.62 ± 0.09^b	$0.90 \pm 0.01^{b,c}$	1.10 ± 0.01^b
5.0	0.62 ± 0.38^b	0.92 ± 0.01^b	1.12 ± 0.00^b
10.0	0.68 ± 0.27^b	0.89 ± 0.00^c	1.11 ± 0.01^b
100.0	NG	NG	NG
Medium: MMD, Ag Type: nano-Ag			
Concentration (mg/L)	Lag Time (h)	Specific Growth Rate (h^{-1})	Max. OD$_{600}$
0	7.40 ± 0.41^a	0.37 ± 0.01^a	0.35 ± 0.01^a
2.5	$7.85 \pm 0.63^{a,b}$	0.40 ± 0.00^b	0.52 ± 0.00^b
5.0	8.71 ± 0.08^b	0.36 ± 0.01^a	$0.35 \pm 0.03^{a,c}$
10.0	$7.84 \pm 1.14^{a,b}$	0.34 ± 0.02^a	0.30 ± 0.01^c
100.0	$11.24 \pm 1.53^{a,b}$	0.24 ± 0.04^c	0.20 ± 0.02^d
Medium: MMD, Ag Type: AgNO$_3$			
Concentration (mg/L)	Lag Time (h)	Specific Growth Rate (h^{-1})	Max. OD$_{600}$
0	7.40 ± 0.41	0.37 ± 0.01	0.35 ± 0.01
2.5	NG	NG	NG
5.0	NG	NG	NG
10.0	NG	NG	NG
100.0	NG	NG	NG

Table 2. Growth parameters for *P. aeruginosa* cultures exposed to varying nano-Ag and $AgNO_3$ concentrations. NG denotes no growth, thus the parameters could not be calculated for these treatments. Like letters in each column indicate no significant difference (t – test, p > 0.05).

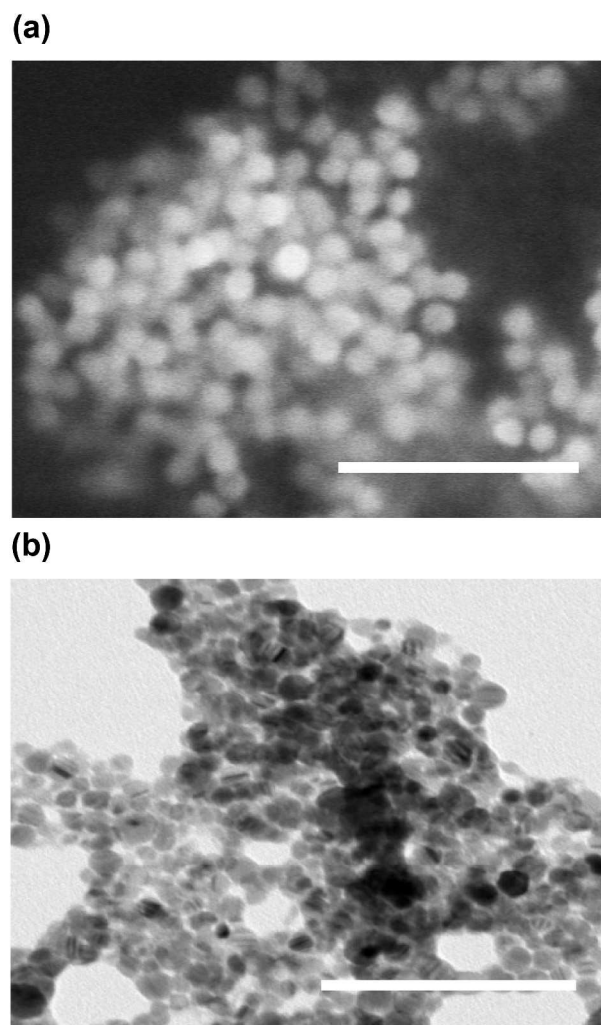| Medium: LB, Ag Type: nano-Ag			
Concentration (mg/L)	Lag Time (h)	Specific Growth Rate (h^{-1})	Max. OD_{600}
0	1.20 ± 0.27^a	0.78 ± 0.02^a	1.35 ± 0.02^a
2.5	$0.77 \pm 0.20^{a,b}$	0.79 ± 0.01^a	1.40 ± 0.00^b
5.0	0.26 ± 0.01^b	0.69 ± 0.01^b	1.39 ± 0.01^b
10.0	0.99 ± 0.10^a	0.66 ± 0.00^c	1.37 ± 0.01^a
100.0	9.24 ± 2.59^c	0.34 ± 0.05^d	1.02 ± 0.01^c
Medium: LB, Ag Type: $AgNO_3$			
Concentration (mg/L)	Lag Time (h)	Specific Growth Rate (h^{-1})	Max. OD_{600}
0	1.20 ± 0.27^a	0.78 ± 0.02^a	1.35 ± 0.02^a
2.5	3.38 ± 0.17^b	0.58 ± 0.01^b	1.34 ± 0.00^a
5.0	NG	NG	NG
10.0	NG	NG	NG
100.0	NG	NG	NG
Medium: MMD, Ag Type: nano-Ag			
Concentration (mg/L)	Lag Time (h)	Specific Growth Rate (h^{-1})	Max. OD_{600}
0	1.60 ± 0.45^a	0.47 ± 0.01^a	0.18 ± 0.02^a
2.5	$3.90 \pm 2.17^{a,b}$	$0.39 \pm 0.06^{a,b}$	0.27 ± 0.01^b
5.0	7.77 ± 0.47^b	0.25 ± 0.00^b	0.10 ± 0.01^c
10.0	NG	NG	NG
100.0	NG	NG	NG
Medium: MMD, Ag Type: $AgNO_3$			
Concentration (mg/L)	Lag Time (h)	Specific Growth Rate (h^{-1})	Max. OD_{600}
0	1.60 ± 0.45	0.47 ± 0.01	0.18 ± 0.02
2.5	NG	NG	NG
5.0	NG	NG	NG
10.0	NG	NG	NG
100.0	NG	NG	NG

(a)

(b)

Figure 1. SEM (a) and TEM (b) micrographs of cysteine coated nano-Ag. The scale bars in each image represent 100 nm.
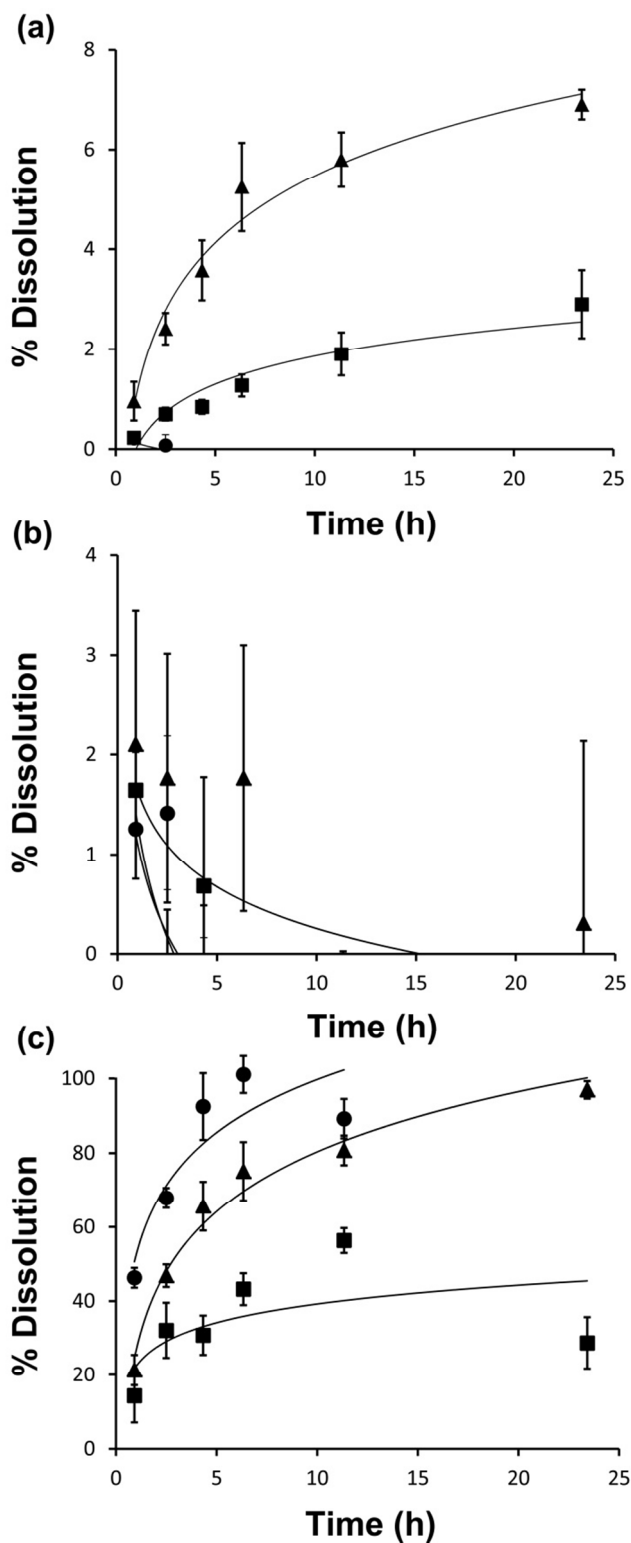
Figure 2. Nano-Ag at 100 mg L^{-1} (a), nano-Ag at 10 mg L^{-1} (b) and AgNO$_3$ at 10 mg L^{-1} (c) dissolution versus time. ●, ■ and ▲ correspond to H$_2$O, MMD and LB media, respectively. Dissolution of nano-Ag at both concentrations was measured over the full time interval (i.e. 24 h), but values were not above background levels. Error bars represent the standard error of the mean.
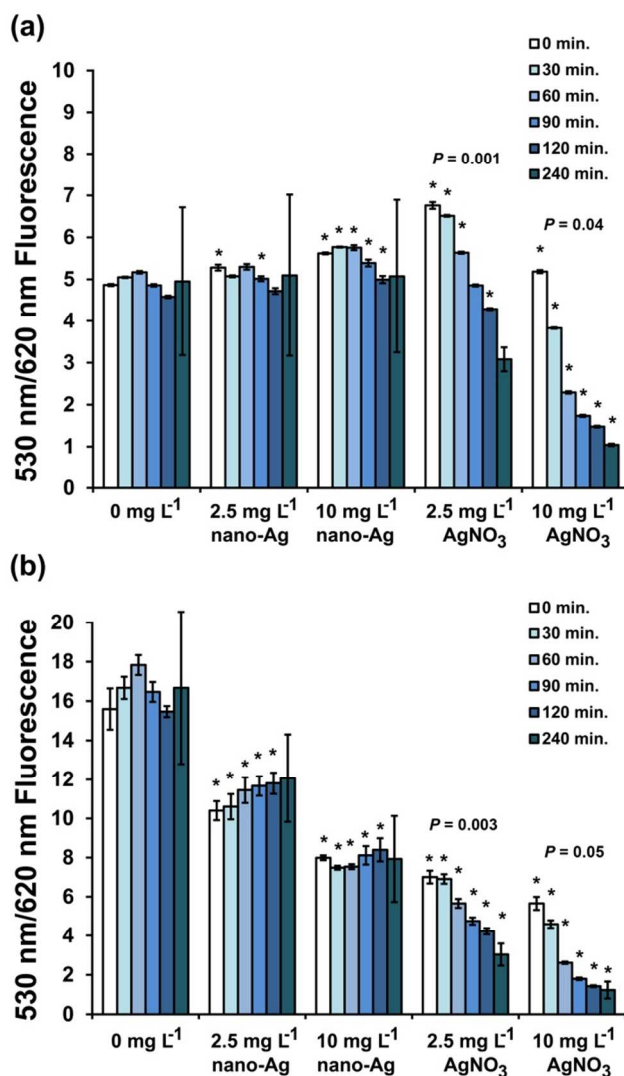
29

Figure 3. Fluorescence ratio (530:620 nm), indicating membrane integrity, for *E. coli* (a) and *P. aeruginosa* (b) in MMD medium amended with nano-Ag or AgNO$_3$. Error bars represent the standard error of the mean. Asterisks (*) indicate values that are significantly different than the control (0 mg L^{-1}) at each time point (*t* test, p < 0.05). For both *E. coli* and *P. aeruginosa*, time significantly affected the fluorescence ratio (two-way ANOVA, p < 0.05) in the AgNO$_3$ treatments. P values for each of these treatments are shown above the respective graphs. For all other treatments, the fluorescence ratio was not affected by time (p > 0.05).
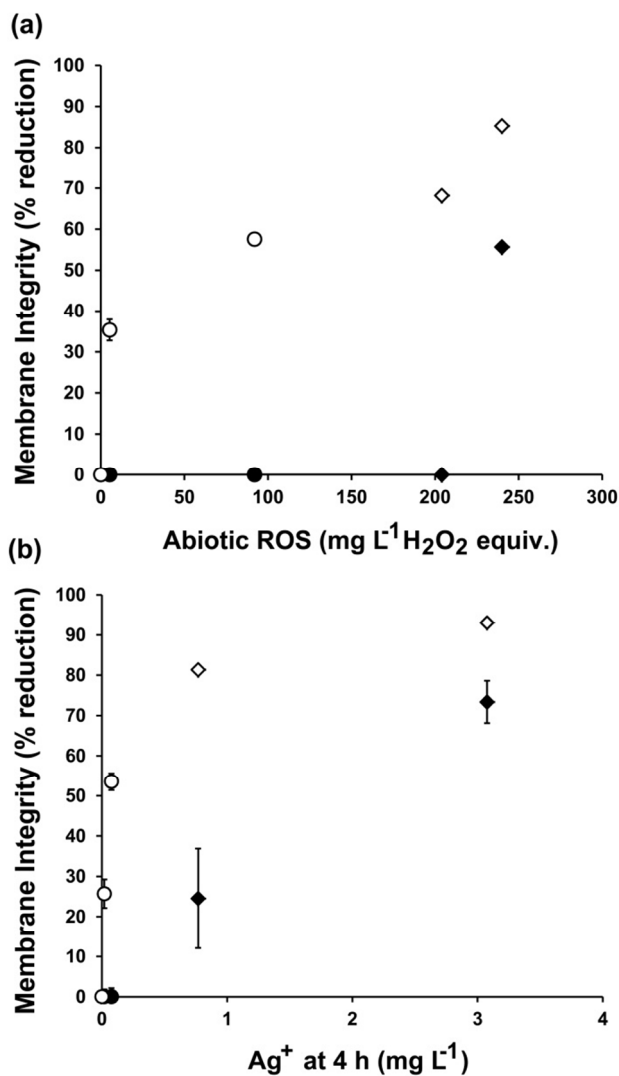
30

Figure 4. Membrane integrity reduction versus abiotic ROS at 1 h (a) and dissolved Ag^+ ion concentration at 4 h (b) for *E. coli* (closed symbols), and *P. aeruginosa* (open symbols). Circles and diamonds represent nano-Ag and $AgNO_3$ treatments, respectively. Error bars represent the standard error of the mean. Where not visible, error bars are smaller than the symbol.
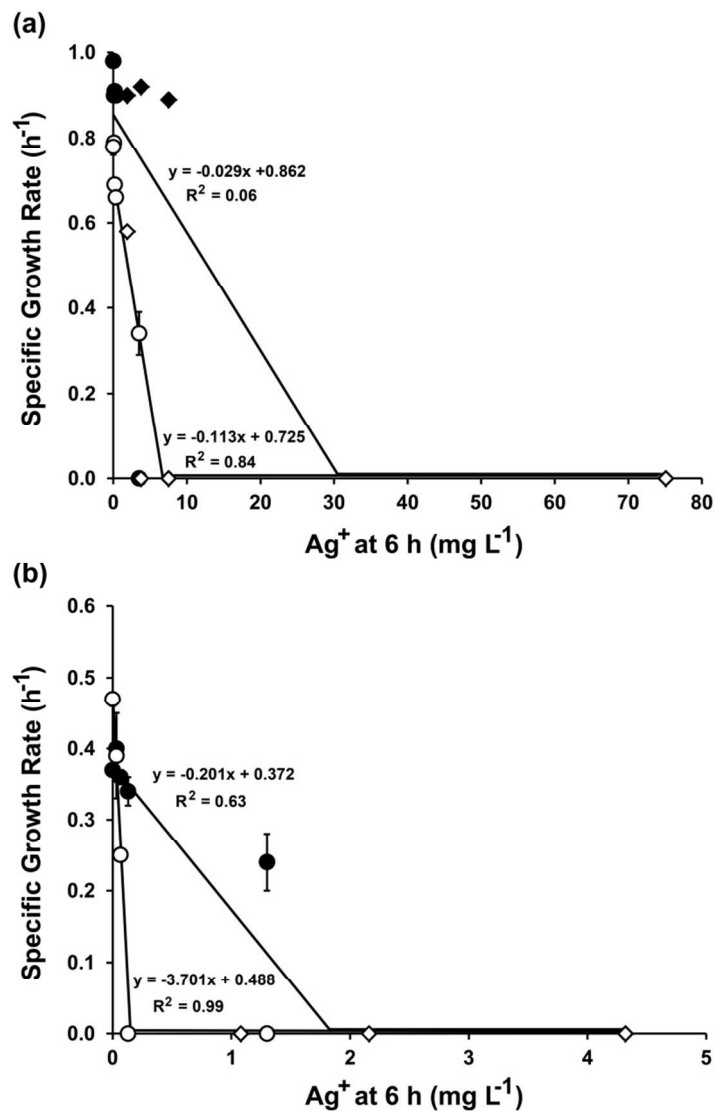
31

(a)

(b)

Figure 5. Specific growth rate of *E. coli* (closed symbols) and *P. aeruginosa* (open symbols) versus 6 h dissolved Ag$^+$ ion concentration in LB (a) and MMD (b). Circles and diamonds represent nano-Ag and AgNO$_3$ treatments, respectively. Error bars represent the standard error of the mean.

32